



Article

Synthesis, Structure, and Luminescence Properties of Zinc(II) Complex with a Spacer-Armed Tetradentate N₂O₂-Donor Schiff Base

Alexey Gusev ¹, Elena Braga ¹, Kirill Mamontov ¹, Mikhail Kiskin ²  and Wolfgang Linert ^{3,*} 

¹ General Chemistry Department, Crimean Federal University V.I. Vernadsky, 295007 Simferopol, Russia; galex0330@gmail.com (A.G.); braga.yelena@ya.ru (E.B.); pro100_keri4@mail.ru (K.M.)

² N.S. Kurnakov Institute of General and Inorganic Chemistry, Russian Academy of Sciences, 119991 Moscow, Russia; mkiskin@igic.ras.ru

³ Institute of Applied Physics, Vienna University of Technology, Wiedner Hauptstraße 8-10, 1040 Vienna, Austria

* Correspondence: wolfgang.linert@tuwien.ac.at; Tel.: +43-1-58801-163613

Abstract: A zinc complex bearing a pyrazolone-based azomethine ligand has been synthesized for blue-emitting organic light-emitting diodes (OLEDs). The azomethine ligand H₂L and the complex [ZnL·H₂O] were characterized by IR, ¹H NMR, XRD, and TGA/DSC techniques. According to a single-crystal X-ray diffraction analysis, the complex [ZnL·H₂O] has a molecular structure. Its solid-state PL maxima appear to be at 416 nm and emit moderate blue emission with a quantum yield (QY) of 2%, with a dehydrated form of the complex showing greater efficiency with a QY of 55.5%. ZnL-based electroluminescent devices for OLED applications were fabricated. The devices exhibit blue emission with brightness up to 5300 Cd/A.

Keywords: Zn(II) complex Schiff base; pyrazolone; photoluminescence; OLEDs



Academic Editor: Santo Di Bella

Received: 14 April 2025

Revised: 13 May 2025

Accepted: 14 May 2025

Published: 19 May 2025

Citation: Gusev, A.; Braga, E.; Mamontov, K.; Kiskin, M.; Linert, W. Synthesis, Structure, and Luminescence Properties of Zinc(II) Complex with a Spacer-Armed Tetradentate N₂O₂-Donor Schiff Base. *Inorganics* **2025**, *13*, 173. <https://doi.org/10.3390/inorganics13050173>

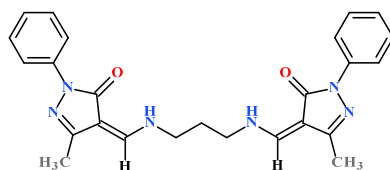
Copyright: © 2025 by the authors. Licensee MDPI, Basel, Switzerland. This article is an open access article distributed under the terms and conditions of the Creative Commons Attribution (CC BY) license (<https://creativecommons.org/licenses/by/4.0/>).

1. Introduction

Since the beginning of the 21st century, organic light-emitting diodes (OLEDs) have been actively researched not only from a fundamental point of view but also in the direction of commercialization in applications for smartphone displays and large-screen high-definition televisions. OLED displays are also expected to become the next generation of lighting technology due to their advantages of surface emitting, lightness, and flexibility [1–5]. The high efficiency of OLED devices has been achieved through the development of phosphorescent and thermally activated fluorescence-delayed emitters, which can use triplet excited states for emission, which are usually dark due to charge injection [6–8]. Until recently, the most effective OLEDs were obtained on the basis of rare and expensive metals (iridium, platinum, gold) [9–13] or on the basis of rather complex organic molecules [4] that degrade quite quickly during the operation of devices. Thus, the high cost and/or short lifespan of the devices hinder the commercialization of electroluminescent devices. Thus, there is an urgent necessity to develop a strategy for designing luminescent compounds to create stable OLED emitters that can replace the use of organic phosphors as well as a platinum group of metals and still provide efficient blue luminescence [14,15].

Recently, our group described relatively simple zinc coordination compounds incorporating pyrazolone-based azomethine ligands, which demonstrate record brightness and blue electroluminescence efficiency [16–19]. Using this approach to continue the search for

effective emitters, in this article, we present the results of comprehensive investigations of the structure, photo- and electro-luminescent properties of zinc Schiff base complex, derived from propane-1,3-diamine with 3-methyl-1-phenyl-4-formylpyrazol-5-one ligand H_2L used in this study (Scheme 1).



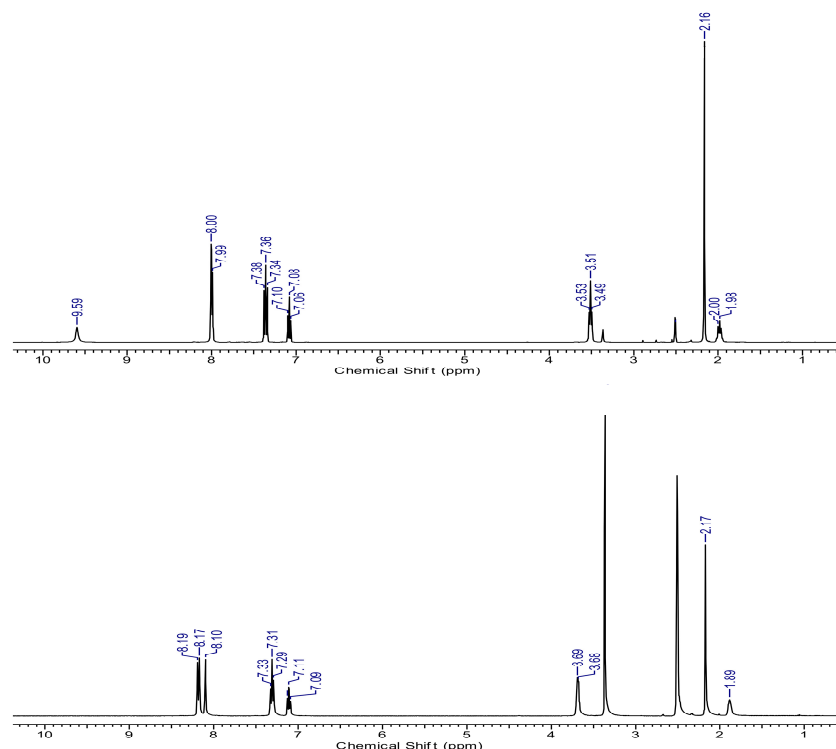
Scheme 1. Structure of azomethine ligand.

2. Results

2.1. Structure of Ligand and Zinc Complex

We have previously described the fluorescent properties of the ZnL complex in solutions [20]. Since high luminescence efficiency in the solid state is required to evaluate the possibility of using zinc complexes as emitters in OLED devices, the present paper presents the results of the study structure and properties in the solid state.

An analysis of the literature data shows that azomethine derivatives of 4-acyl-3-methyl-1-phenylpyrazol-5-ones can exist in four tautomeric forms [21], of which the imino-ol (B) and the amine-one forms (A) are the most stable Scheme 2. A comparative analysis of NMR spectroscopy of the ligand and the complex testifies to the transition of the A form to the B form during complexation with zinc cation in alkaline medium (Figure 1). The most indicative is the disappearance of the “acidic” proton of the NH group registered in the azomethine spectrum at 9.59 ppm and the appearance of the singlet signal of the aldehyde proton in the complex spectrum at 8.10 ppm. The number of peaks observed in the 1H NMR spectrum of the complex is consistent with the total number of hydrogen atoms present in the structure, which indicates stability of the complex in solution.



Scheme 2. Tautomeric equilibria and the synthetic route for the synthesis of the zinc complex.

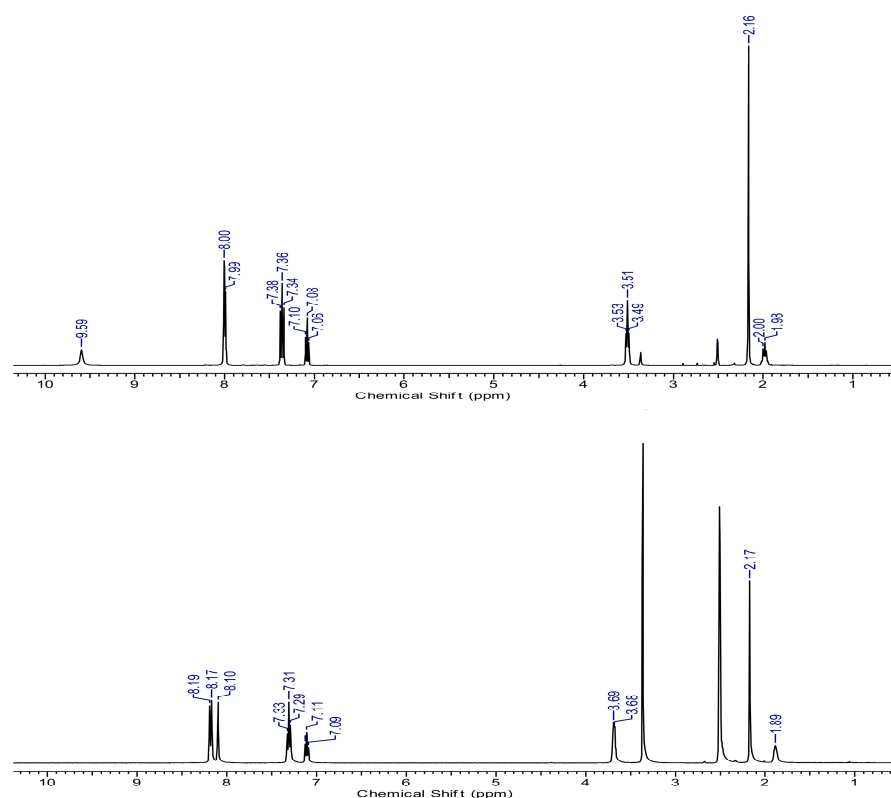


Figure 1. The ^1H NMR spectrum of complex (**below**) and azomethine ligand (**above**).

The spectral data are in high agreement with the data of X-ray analysis of single crystals of azomethine and the complex (Table S1). Needle-like crystals of the ligand were obtained by recrystallization from methanol. The compound crystallizes in the monoclinic space group $P2_1/n$. The molecular structure of H_2L with the atom numbering scheme is shown in Figure 2. The presence of the ligand in the amine-one form is confirmed by the analysis of the bond length. In particular, the bond lengths of $\text{O}=\text{C}$ (1.236(3) Å) and 1.244(3) Å demonstrate that the oxygen atoms of the carbonyl are in the keto form. The bond length values of $\text{C}10\text{--C}12/\text{C}18\text{--C}21$ (1.386(4) and 1.376(4) Å) and $\text{C}12\text{--N}3/\text{C}18\text{--N}6$ (1.305(4) and 1.312(3) Å) distances are intermediate between those for single and double $\text{C}=\text{C}$ ($\text{C}=\text{N}$) bonds, which is explained by their incorporation into the conjugated system. The hydrogen atoms of the NH group are involved in bifurcate hydrogen bonds with the oxygen atoms of their own and neighboring molecules (see Table S2), leading to the formation of a 1D helical supramolecular structure. The crystal structure is stabilized by $\text{C}\text{--H}\cdots\text{O}/\text{N}/\pi$ and $\pi\cdots\pi$ intermolecular interactions (see Tables S2–S4).

The molecular complex $\text{ZnL}\cdot\text{H}_2\text{O}$ crystallizes in a triclinic system with space group $P\bar{1}$ (Figure 3, Table S5). The coordination environment of the Zn atom is formed by $\text{O}2$, $\text{O}3$, $\text{N}3$, and $\text{N}4$ atoms from one double-deprotonated azomethine ligand L^{2-} and one oxygen atom ($\text{O}5$) of the water molecule, forming a distorted trigonal bipyramidal geometry ($\tau_5 = 0.72$) [22]. The atoms $\text{O}1$, $\text{O}3$, and $\text{N}4$ form the equatorial plane, and the Zn atom deviates from the equatorial plane by 0.028 Å. The axial positions are occupied by the atoms $\text{O}2$ and $\text{N}3$ from the ligand. In addition, the bond lengths of $\text{O}1\text{--C}3$ (1.2761(16) Å) and $\text{O}2\text{--C}19$ (1.2691(16) Å) indicate that the oxygens of the carbonyls take part in coordination through the enolic form, and their active hydrogen is replaced by the Zn(II) ion. Parameters of chemical bonds of the coordination polyhedron are given in Table S2. In the crystal structure, there are significant intermolecular bonding interactions between the molecules. Intermolecular hydrogen bonds between the coordinated water molecules and the nitrogen atoms of the pyrazolone ring of the ligand anion (Table S2) are formed between every

two molecules, linking the neighboring molecules to a supramolecular chain, as shown in Figure 3b. Furthermore, each molecule is held together by $\pi\cdots\pi$ stacking interactions between neighboring pyrazole rings (Table S4).

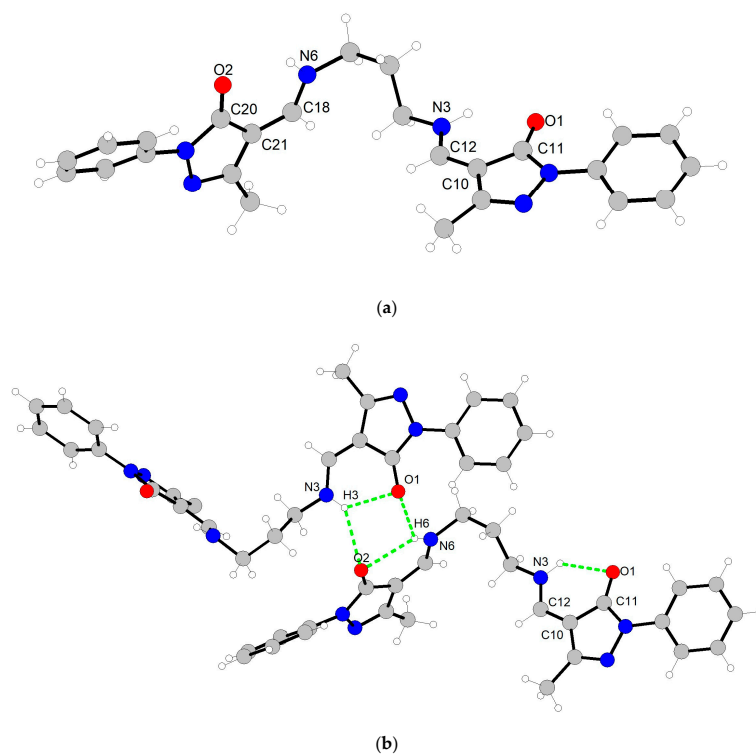


Figure 2. (a) Molecular structure of H_2L ; (b) intermolecular H-bonding between H_2L .

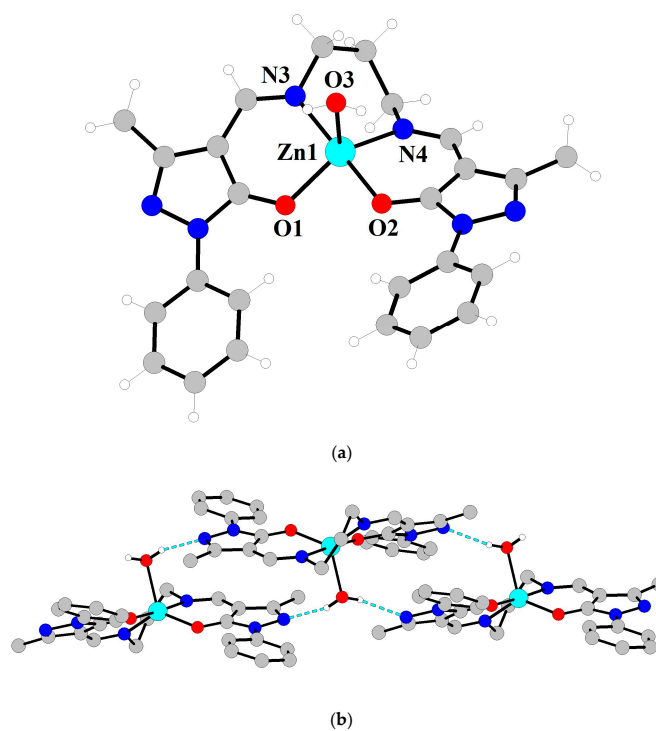


Figure 3. (a) Molecular structure of $ZnL \cdot H_2O$; (b) intermolecular hydrogen bonding between neighboring complex molecules.

Since thermal stability is one of the most important characteristics of photoactive compounds, thermal studies of the complex by TGA and DSC methods were performed (Figure 4). The complex is stable up to a temperature of 192 °C. Then, in the interval 192–258 °C, there is a loss of 3.51% of mass due to the removal of the coordinated water molecule (calc. 3.44%). Dehydration of the sample is accompanied by an endothermic effect with a minimum of the DSC curve at 241 °C. The desolvated complex is stable up to a temperature of 425 °C, above which partial sublimation starts (accompanied by an endothermic effect with a minimum of the DSC curve at 455 °C), transforming into decomposition of the sample.

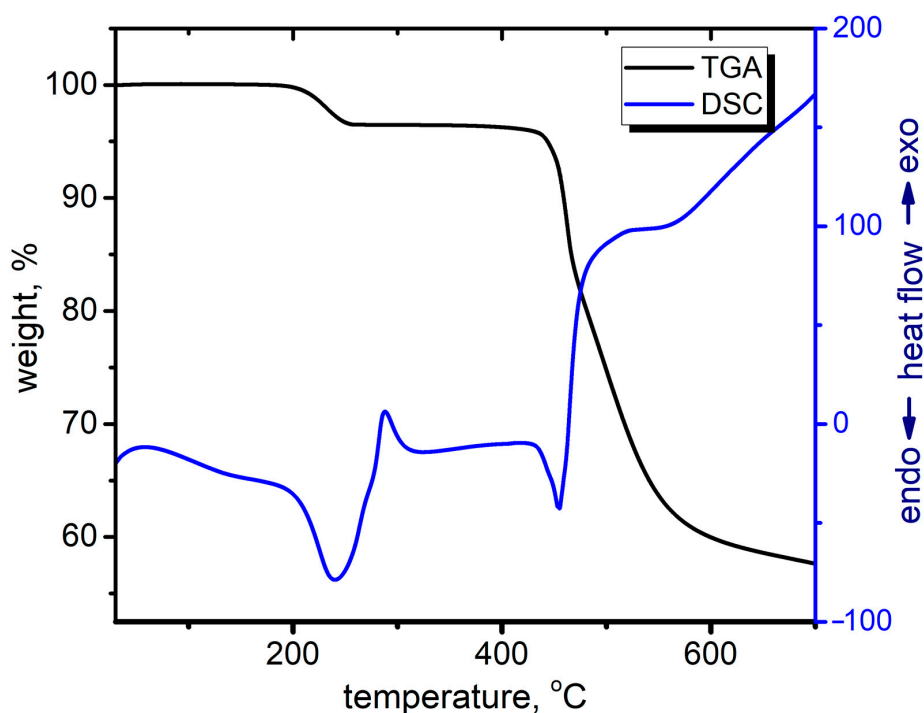


Figure 4. TG and DSC curves of zinc complex.

2.2. Photophysical Properties of Zinc Complex

Previously, we presented the results of a study of the photophysical properties of the complex in solution [20]. However, for the use of luminescent complexes as emitting layers in OLEDs, data on the optical properties in the solid state are needed. Thus, in the present work, we focused on the study of photophysical characteristics for the zinc complex in crystal and powder states. Figure 5 shows the absorption spectra of the title Schiff base and zinc complex.

It is found that H_2L exhibits two distinct absorption bands at 240 and 282 nm. These absorption bands can be assigned to the $\pi-\pi^*$ and $n-\pi^*$ transitions of $C=C/C=N$ and $C=O$ chromophores, respectively. The addition of zinc cation and the transition of the ligand to the deprotonated form in the complex $ZnL \cdot H_2O$ are accompanied by a bathochromic shift in the corresponding bands to 265 (shoulder) and 292 nm, respectively. In addition, in the region of 330–400 nm, a broad band is registered, which we assigned to the metal–ligand charge transfer [23–25].

Under UV lamp exposure, the crystals of the $ZnL \cdot H_2O$ show weak blue photoluminescence with CIE coordinates of 0.16, 0.16. The optimal excitation wavelength was selected from the excitation spectrum and is 345 nm. The emission spectrum has a broad asymmetric band form with a main maximum at 416 nm and a shoulder at 470 nm (Figure 6). The appearance of additional bands in the red region of the spectrum was previously observed

for the complex with a dimethylene spacer, and their appearance was attributed to excimer emission [17].

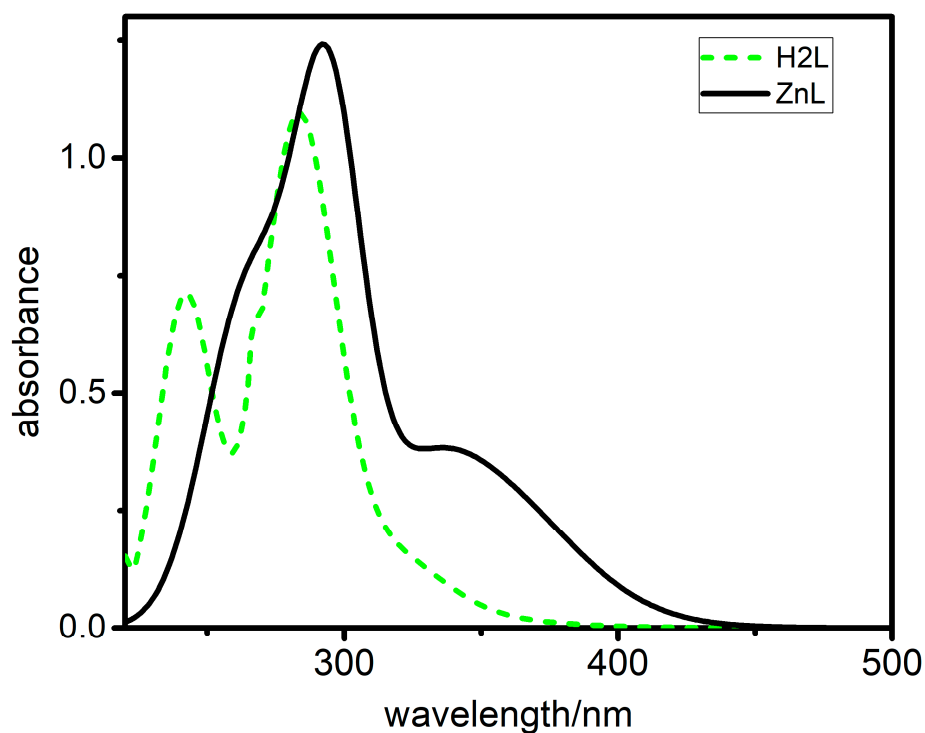


Figure 5. The absorption profiles of solid-state H_2L and $ZnL \cdot H_2O$.

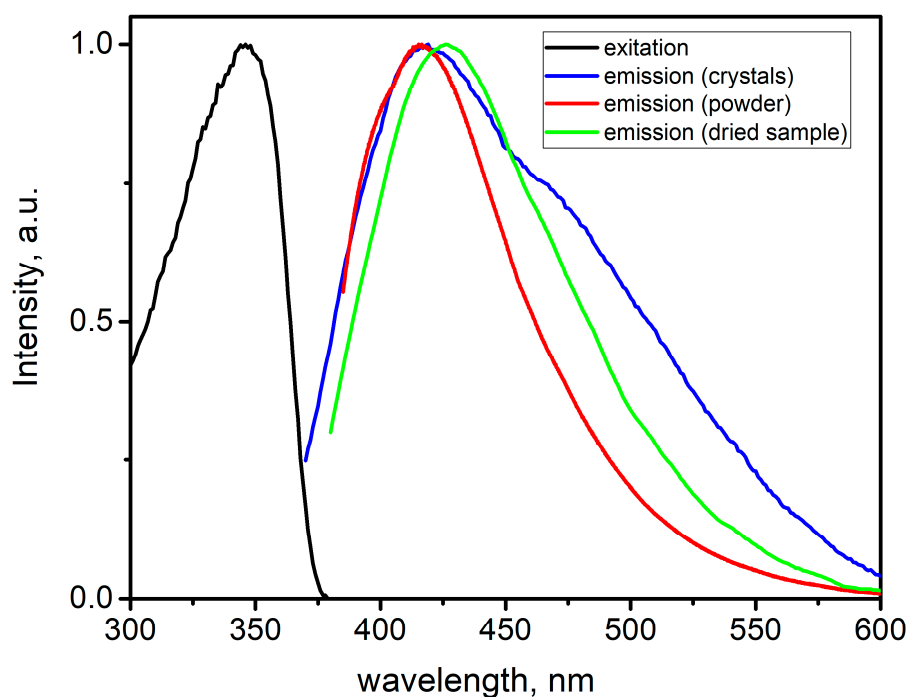


Figure 6. The excitation and emission of the zinc complex in different states.

Taking into account the close structure of the title complex and the previously described one, the appearance of the shoulder at 470 nm is also obviously related to excimer luminescence. Compared to the previously described spectrum of the complex in solution [20], the maximum in the solid is hypsochromically shifted. Moreover, only one maximum was registered at low concentrations in solution, which is additional evidence

of the excimeric nature of the signal at 470 nm registered in the study of crystals. Further studies showed that careful grinding of the complex leads to the disappearance of the excimer signal, indicating the role of intermolecular interactions in the realization of excimer luminescence. The molecular and crystalline structure is preserved during grinding, which is confirmed by the data of an X-ray diffraction analysis of the powder (Figure S1). It is noteworthy that the quantum yield of luminescence for both the crystalline sample and the ground sample is only 2% and 4.1%, respectively. Considering the presence of a coordinated water molecule in the structure of the complex, we believed that the low emission efficiency of the crystalline sample is associated with non-radiative losses of excitation energy, which leads to the quenching of luminescence [26]. Based on the data of thermal analysis of the complex, we prepared an anhydrous sample of the complex by heating and keeping it for one hour at 250 °C followed by recrystallization from benzene. Complete removal of the coordinated water molecule was confirmed by elemental and thermal analyses and IR spectroscopy (Figures S2 and S3). The dehydrated complex exhibits brilliant blue luminescence with CIE1931 (Commission Internationale de l'Éclairage) coordinates of 0.16, 0.12 under excitation at 350 nm. The luminescence spectrum has the shape of a broad band with one maximum. The emission maximum of the dehydrated complex is shifted to 427 nm, and the quantum yield increases to 55.5%. This fact confirms the quenching effect of the water molecule. Additionally, dehydration of the complex affects the decay lifetime as well. The decay curve of the hydrated complex is approximated by a biexponential function

$$y = A_1 \exp(-x/\tau_1) + A_2 \exp(-x/\tau_2)$$

with the best-fit parameters of $\tau_1 = 6.8$ ns, $A_1 = 0.32$; $\tau_2 = 12.0$ ns, $A_2 = 0.68$, while the decay of the dehydrated compound is well fitted by a monoexponential function with the τ value of 10.1 ns. The biexponential character of crystal emission attenuation is consistent with the luminescence spectrum of a crystal sample, which is a superposition of monomeric and excimeric signals; therefore, it is more correct to use a biexponential curve reflecting two pathways of deactivation of the excited state.

According to the literature, zinc Schiff base complexes with azomethine ligands have shown tremendous interest as emissive materials in OLEDs [27]. Our studies have shown that the dehydrated synthesized complex, due to its high thermal stability and high efficiency of blue luminescence, is an ideal candidate for the creation of blue electroluminescent devices, so the electroluminescence properties of the complex as emissive layers were tested in the following fabricated OLED structures.

2.3. Electroluminescence Performance

To verify the hypothesis about the possibility of using a zinc complex as emitters in electroluminescent devices, we have constructed and characterized three devices of the following structure: ITO/MoO₃/NPB/(complex + host matrix)/TSPO1/TPBi/LiF/Al. Here, we used the combination of ITO/MoO₃/NPB as the hole-injection layer. TSPO1, TPBi, and LiF were used as hole blocking, electron-transport layers, and electron-injection material, respectively, for providing an optimal balance of the charge carriers in the emissive layer. The non-doped device demonstrated poor electroluminescent brightness, which might be attributed to uneven charge carrier injection and transportation in the emissive layer [28], so we used the obtained complex as emitting dopants with 5% weight doping concentrations to the relevant host matrix [29]. The choice of host matrixes (mCp-1,3-Bis(carbazol-9-yl)benzene (Device A); PYD-2Cz-2,6-di(9H-carbazol-9-yl)pyridine) (Device B); and CBP-4,4'-bis(carbazol-9-yl)biphenyl (Device C) was determined by the ratio of HOMO-LUMO energies of neighboring layers and the complex matching HOMO-LUMO energy level to that of emitter molecules providing carrier transporting characteristics, good

film-forming properties, and high thermal stability. The energy of HOMO/LUMO orbitals was determined yearly by the measurements of optical spectra and cyclic voltammetry [20].

The schematic energy-level diagram in the eV of OLED devices fabricated in this work is shown in Figure 7. The electroluminescence spectra of the devices A-C and the characteristics of the devices are shown in Figure 8 and also provided in Table 1.

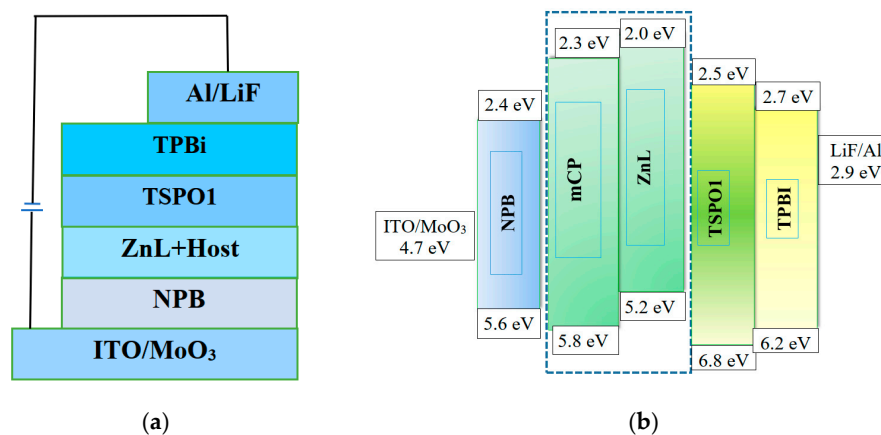


Figure 7. (a) Device structures of OLEDs A–C; (b) schematic energy-level diagram of device A.

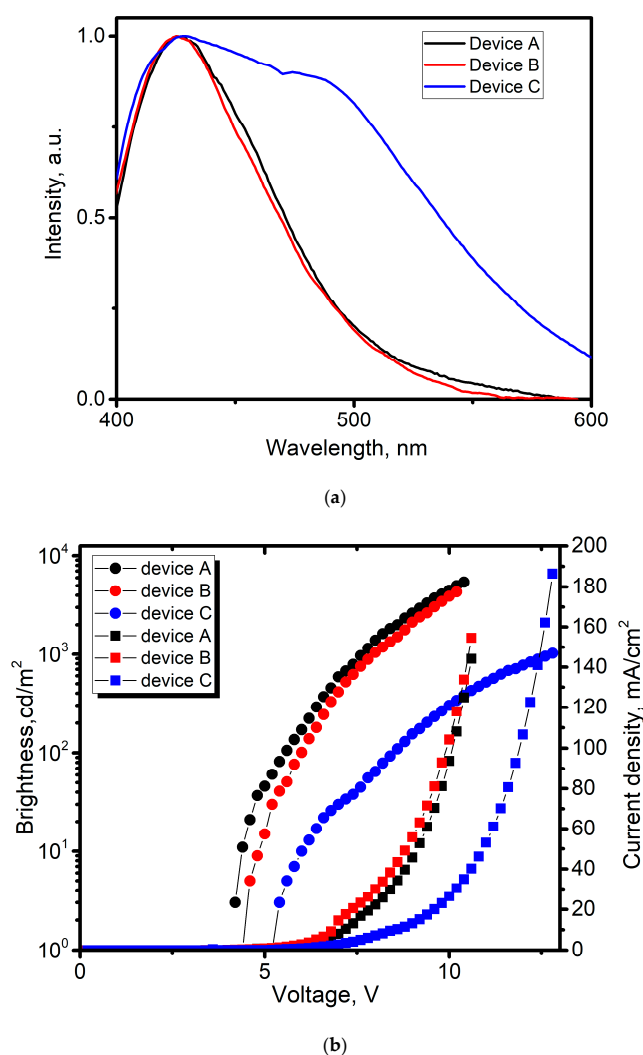


Figure 8. Cont.

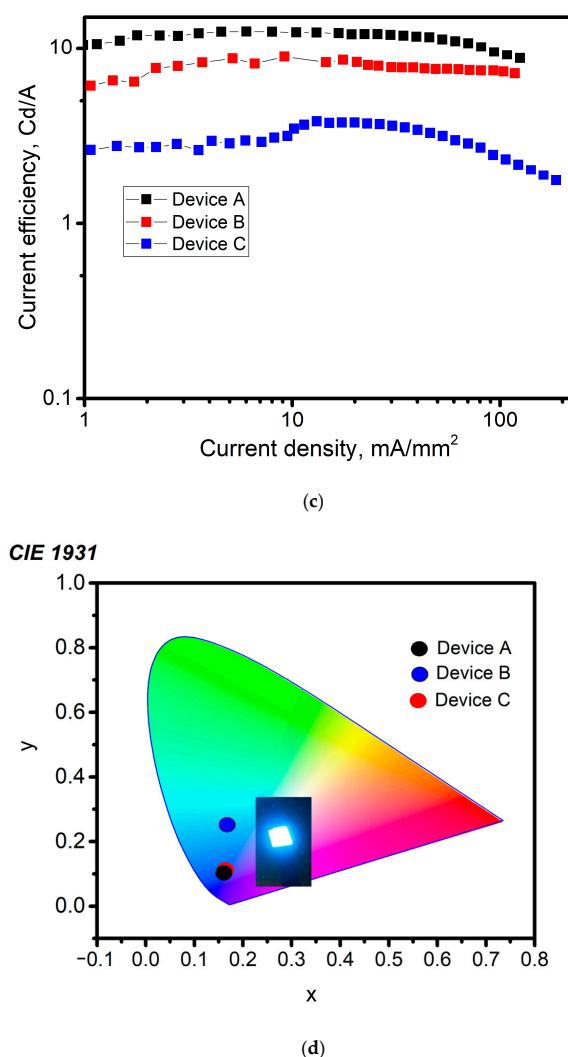


Figure 8. (a) Normalized electroluminescence spectra of devices A–C at 7 V. (b) Current density–voltage–brightness characteristics of devices A–C. (c) Current efficiency of devices A–C. (d) CIE coordinates of emission for devices A–C. Inset—photo of working devices A and B.

Table 1. Electroluminescence characteristics of devices A–C.

Compounds	Turn-On Voltage (V)	Luminance (cd/m ²)	CIE Coordinates	CE (cd/A)	EQE (%)
A	4.2	5430	0.1552, 0.1405	12.4	4
B	4.4	4320	0.1578, 0.1540	8.9	3.1
C	5.2	1020	0.1532, 0.2306	3.8	1.5

As can be seen from Figure 8a, the EL emission band for devices A and B remains similar to the PL spectrum of the crystalline sample. There is no luminescence from the electroplexes implying that these devices are effective. EL spectra show a single peak located at 425 nm and 426 nm, demonstrating deep-blue electroluminescence with CIE 1931 (0.1552, 0.1405) and (0.1578, 0.1540), which is very close to the NTSC standard blue value (0.14, 0.08). In the case device C, in addition to the main signal of the complex at 425 nm, the electroluminescence spectrum shows an additional peak at 478 nm due to excimer emission, indicating an efficient Förster energy transfer from the host CBP molecules to the molecules of the complex. CIE coordinates for device C are 0.1532, 0.2306. Among the three devices, device A achieved the best electroluminescent performances

with a maximum brightness of 5400 Cd/m², a CE (current efficiency) of 12.4 cd/A, and an EQE (external quantum efficiency) of 4.02%. This result could be the reason for the more efficient exciton recombination process and host–guest energy transfer. For zinc-complex blue emitters, this performance is quite high but non-recorded [16,30], probably due to the device’s constructive imperfection, an unsuitable thickness of layers, and the mismatching energy level of materials. Anyway, the present investigation demonstrates the utilization of the zinc complex as an emissive material to construct efficient high high-luminance blue OLEDs.

3. Materials and Methods

All the reagents and solvents were commercially available (Khimmed (Moscow, Russia), analytical grade) and used as received without further purification. Title azomethine and Zinc complex were prepared according to the method used in the study of [20].

Diffuse reflectance spectra were recorded with a Cintra-3000 spectrophotometer for the solid-state samples. ¹H NMR spectra were recorded on a Bruker VXR-400 spectrometer at 400 MHz using the DMSO-d₆ solutions. Photoluminescence and excitation spectra were recorded on the Fluorolog FL3-22 spectrometer for the complex in solid state. Luminescence decays were measured using the same spectrometer equipped with a xenon flash lamp. The luminescence quantum yields of the solid samples were determined by the absolute method using an integrating sphere. The thermal behavior of complex was studied using the simultaneous thermal analysis (STA) technique for parallel recording of TG (thermogravimetry) and DSC (differential scanning calorimetry) curves.

The single crystal X-ray diffraction data were collected using the SuperNova diffractometer equipped with an Atlas detector and a micro-focus CuK α radiation source ($\lambda = 1.54184 \text{ \AA}$) for H₂L and the Bruker D8 Venture diffractometer equipped with a CCD detector and a micro-focus MoK α radiation source ($\lambda = 0.71073 \text{ \AA}$) for ZnL·H₂O. Semi-empirical absorption correction was applied for both samples [31]. The structures were solved by the direct methods and refined in the full-matrix anisotropic approximation for all non-hydrogen atoms. The hydrogen atoms of oxygen and nitrogen atoms were found in differential Fourier maps, and their parameters were refined using the riding model. The hydrogen atoms of the carbon-containing ligand were positioned geometrically and refined by using a riding model. All the calculations were performed by direct methods and using the SHELX-2018 and OLEX-2 program package [32,33]. The crystallographic parameters and the structure refinement statistics are shown in Table S1. CCDC numbers 2,434,148 (for H₂L) and 2,434,149 (for ZnL·H₂O) contain the supplementary crystallographic data for the reported compounds. These data can be obtained free of charge from The Cambridge Crystallographic Data Centre via http://www.ccdc.cam.ac.uk/data_request/cif (accessed on 25 March 2025).

OLED Preparation

Fabrication of the OLED performed according to the methodology described earlier [18]: using “AUTO 306” equipment by “BOC EDWARDS” (Crawley, UK) for thermal deposition of layers sand quartz detector SQM 160 (INFICON GmbH, New York, NY, USA) for control of evaporation speed and thickness of the deposited layers.

The voltage–current and luminance measurements of the obtained OLED structures were studied on a measuring complex consisting of a voltage analyzer source (Keithley 237, KEITHLEY, Cleveland, OH, USA) and a fiber spectrometer (AvaSpec-ULS-2048 × 64, Avantes BV, Apeldoorn, The Netherlands).

4. Conclusions

The structure of the new Salen-type tetradentate N₂O₂ azomethine chelate ligand 5-methyl-4-[[3-[[[(3-methyl-5-oxo-1-phenyl-pyrazol-4-ylidene)methyl]amino]propylamino]methylene]-2-phenyl-pyrazol-3-one and zinc complex on its basis was investigated. Spectral and diffraction methods revealed that, during the reaction, the tautomeric form of the ligand changes from amino to deprotonated iminol form. The complex has a mononuclear structure with a pentacoordinated zinc cation. Moreover, the solid-state photoluminescent properties reveal that the Zn(II) complex in crystalline form exhibited a weak blue luminescence (QY about 2%), while the dehydrated complex demonstrates strong emission with QY 55%. The electroluminescence characteristics of the zinc complex-based OLED devices were studied. The maximum current efficiency of 12.4% and maximum luminance of 5430 cd/m² were achieved.

Supplementary Materials: The following supporting information can be downloaded at <https://www.mdpi.com/article/10.3390/inorganics13050173/s1>. Table S1: Crystal data and structure refinements for H₂L and ZnL·H₂O; Table S2: D-H···A interactions in crystals of H₂L and ZnL·H₂O; Table S3: C–X···π interactions in H₂L and ZnL·H₂O; Table S4: Selected parameters of π...π intermolecular interactions in H₂L and ZnL·H₂O; Table S5: Selected geometric parameters for ZnL·H₂O; Figure S1: PXRD diffractograms of grounded crystals of zinc complex; Figure S2: IR spectra of hydrated (black line) and unhydrated (red line) zinc complex and elemental analysis data for unhydrated sample; Figure S3: TGA curve of unhydrated zinc complex.

Author Contributions: A.G.—Conceptualization, methodology, supervision, and writing—original draft preparation; E.B.—Validation, investigation, and formal analysis; K.M.—validation, investigation, and formal analysis; M.K.—Validation, investigation, and formal analysis; W.L.—Investigation, project administration, and writing—review and editing; All authors have read and agreed to the published version of the manuscript.

Funding: The authors would like to acknowledge the financial support from the Russian Science Foundation grant (25-23-00143).

Data Availability Statement: Samples of the compounds are available from the authors.

Acknowledgments: M. Kiskin thanks the state assignment of the IGIC RAS in the field of fundamental scientific research for the possibility to perform X-ray diffraction analyses.

Conflicts of Interest: The authors declare no conflicts of interest.

References

1. Nayak, D.; Bilash, R. Choudhary, A survey of the structure, fabrication, and characterization of advanced organic light emitting diodes. *Microelectron. Reliab.* **2023**, *144*, 114959. [\[CrossRef\]](#)
2. Hong, G.; Gan, X.; Leonhardt, C.; Zhang, Z.; Seibert, J.; Busch, J.M.; Bräse, S.; Hong, G.; Gan, X.; Leonhardt, C.; et al. A Brief History of OLEDs—Emitter Development and Industry Milestones. *Adv. Mater.* **2021**, *33*, 2005630. [\[CrossRef\]](#) [\[PubMed\]](#)
3. Tankeleviciūte, E.; Samuel, I.D.W.; Zysman-Colman, E. The Blue Problem: OLED Stability and Degradation Mechanisms. *J. Phys. Chem. Lett.* **2024**, *15*, 1034–1047. [\[CrossRef\]](#)
4. Lee, J.-H.; Chen, C.-H.; Lee, P.-H.; Lin, H.-Y.; Leung, M.; Chiu, T.-L.; Lin, C.-F. Blue organic light-emitting diodes: Current status, challenges, and future outlook. *J. Mater. Chem. C* **2019**, *7*, 5874–5888. [\[CrossRef\]](#)
5. Xia, S.C.; Kwong, R.C.; Adamovich, V.I.; Weaver, M.S.; Brown, J.J. OLED Device Operational Lifetime: Insights and Challenges. In Proceedings of the 2007 IEEE International Reliability Physics Symposium Proceedings. 45th Annual, Phoenix, AZ, USA, 15–19 April 2007; pp. 253–257.
6. Iwasaki, H.; Majima, Y.; Izawa, S. Low-voltage turn-on in blue organic light-emitting diodes. *Synth. Met.* **2024**, *309*, 117772. [\[CrossRef\]](#)
7. Marques dos Santos, J.; Hall, D.; Basumatary, B.; Bryden, M.; Chen, D.; Choudhary, P.; Comerford, T.; Crovini, E.; Danos, A.; De, J.; et al. The Golden Age of Thermally Activated Delayed Fluorescence Materials: Design and Exploitation. *Chem. Rev.* **2024**, *124*, 13736–14110. [\[CrossRef\]](#)

8. Tao, Y.; Yuan, K.; Chen, T.; Xu, P.; Li, H.; Chen, R.; Zheng, C.; Zhang, L.; Huang, W. Thermally activated delayed fluorescence materials towards the breakthrough of organoelectronics. *Adv. Mater.* **2014**, *26*, 7931–7958. [[CrossRef](#)]
9. Jayabharathi, J.; Thanikachalam, V.; Thilagavathy, S. Phosphorescent organic light-emitting devices: Iridium based emitter materials—An overview. *Coord. Chem. Rev.* **2023**, *483*, 215100. [[CrossRef](#)]
10. Tao, P.; Lü, X.; Zhou, G.; Wong, W.-Y. Asymmetric Tris-Heteroleptic Cyclometalated Phosphorescent Iridium(III) Complexes: An Emerging Class of Metallophosphors. *Acc. Mater. Res.* **2022**, *3*, 830–842. [[CrossRef](#)]
11. Gao, H.; Qian, M.; Yang, X.; Ma, S.; Li, H. Recent advances of the cyclometalated iridium(III) complexes for electrochemiluminescence sensing. *Dye. Pigment.* **2025**, *232*, 112493. [[CrossRef](#)]
12. Williams, J.A.G.; Develay, S.; Rochester, D.L.; Murphy, L. Optimising the luminescence of platinum (II) complexes and their application in organic light emitting devices (OLEDs). *Coord. Chem. Rev.* **2008**, *252*, 2596–2611.
13. Tang, M.-C.; Chan, A.K.-W.; Chan, M.-Y.; Yam, V.W.-W. Platinum and Gold Complexes for OLEDs. *Top. Curr. Chem.* **2016**, *374*, 46. [[CrossRef](#)] [[PubMed](#)]
14. Giobbio, G.; Costa, R.D.; Gaillard, S. Earth Abundant Transition Metals Complexes in Light-emitting Electrochemical Cells: Successes, Challenges and Perspectives. *Dalton Trans.* **2025**, *54*, 3573–3580. [[CrossRef](#)]
15. Bizzarri, C.; Spuling, E.; Knoll, D.M.; Volz, D.; Bräse, S. Sustainable metal complexes for organic light-emitting diodes (OLEDs). *Coord. Chem. Rev.* **2018**, *373*, 49–82. [[CrossRef](#)]
16. Gusev, A.N.; Kiskin, M.A.; Braga, E.V.; Kryukova, M.A.; Baryshnikov, G.V.; Karaush-Karmazin, N.N.; Minaeva, V.A.; Minaev, B.F.; Ivaniuk, K.; Stakhira, P.; et al. Schiff Base Zinc(II) Complexes as Promising Emitters for Blue Organic Light-Emitting Diodes. *ACS Appl. Electron. Mater.* **2021**, *3*, 3436–3444. [[CrossRef](#)]
17. Gusev, A.N.; Kiskin, M.A.; Braga, E.V.; Chapran, M.; Wiosna-Salyga, G.; Baryshnikov, G.V.; Minaeva, V.A.; Minaev, B.F.; Ivaniuk, K.; Stakhira, P.; et al. Novel Zinc Complex with an Ethylenediamine Schiff Base for High-Luminance Blue Fluorescent OLED Applications. *J. Phys. Chem. C* **2019**, *123*, 11850–11859. [[CrossRef](#)]
18. Burlov, A.S.; Vlasenko, V.G.; Milutka, M.S.; Koshchienko, Y.V.; Makarova, N.I.; Lazarenko, V.A.; Trigub, A.L.; Kolodina, A.A.; Zubenko, A.A.; Metelitsa, A.V.; et al. Synthesis, Structure, Spectral-Luminescent Properties, and Biological Activity of Chlorine-Substituted N-[2-(Phenyliminomethyl)phenyl]-4-methylbenzenesulfamide and Their Zinc(II) Complexes. *Int. J. Mol. Sci.* **2022**, *23*, 15259. [[CrossRef](#)]
19. Burlov, A.S.; Vlasenko, V.G.; Milutka, M.S.; Koshchienko, Y.V.; Lazarenko, V.A.; Trigub, A.L.; Kolodina, A.A.; Zubenko, A.A.; Braga, E.V.; Gusev, A.N.; et al. Zinc Complexes of Fluorosubstituted N-[2-(Phenyliminomethyl)phenyl]-4-methylbenzenesulfamides: Synthesis, Structure, Luminescent Properties, and Biological Activity. *Materials* **2024**, *17*, 438. [[CrossRef](#)]
20. Gusev, A.; Shul'gin, V.; Braga, E.; Zamnius, E.; Kryukova, M.; Linert, W. Luminescent properties of Zn complexes based on tetradentate N₂O₂-donor pyrazolone schiff bases. *Dye. Pigment.* **2020**, *183*, 108626–108632. [[CrossRef](#)]
21. Marchetti, F.; Pettinari, R.; Pettinari, C. Recent advances in acylpyrazolone metal complexes and their potential applications. *Coord. Chem. Rev.* **2015**, *303*, 1–31. [[CrossRef](#)]
22. Addison, A.W.; Rao, T.N.; Reedijk, J.; Van Rijn, J.; Verschoor, G.C. Synthesis, Structure, and Spectroscopic Properties of Copper(II) Compounds Containing Nitrogen–Sulphur Donor Ligands; the Crystal and Molecular Structure of Aqua[1,7-Bis(N-Methylbenzimidazol-2'-yl)-2,6-dithiaheptane]Copper(II) Perchlorate. *J. Chem. Soc. Dalton Trans.* **1984**, *7*, 1349–1356. [[CrossRef](#)]
23. Olennikov, V.E.; Zvereva, V.V.; Kriventsov, V.V.; Konchenko, S.N.; Sukhikh, T.S. Molecular Switches Guided by a Reversible Access to Room-Temperature Phosphorescence and ESIPT Fluorescence. *Inorg. Chem.* **2025**, *64*, 6964–6976. [[CrossRef](#)]
24. Massue, J.; Jacquemin, D.; Ulrich, G. Molecular Engineering of Excited-state Intramolecular Proton Transfer (ESIPT) Dual and Triple Emitters. *Chem. Lett.* **2018**, *47*, 1083–1089. [[CrossRef](#)]
25. Padalkar, V.S.; Seki, S. Excited-state intramolecular proton-transfer (ESIPT)-inspired solid state emitters. *Chem. Soc. Rev.* **2016**, *45*, 169–202. [[CrossRef](#)]
26. Maillard, J.; Klehs, K.; Rumble, C.; Vauthey, E.; Heilemann, M.; Fürstenberg, A. Universal quenching of common fluorescent probes by water and alcohols. *Chem. Sci.* **2021**, *12*, 1352–1362. [[CrossRef](#)]
27. Rashmuse, T.J.; Mohlala, R.L.; Coynan, E.M.; Magwa, N.P. A Review: Blue Fluorescent Zinc (II) Complexes for OLEDs—A Last Five-Year Recap. *Molecules* **2023**, *28*, 5272. [[CrossRef](#)]
28. Kumar, D.; Justin Thomas, K.R.; Ching-Chiao, L.; Joue, J.H. Molecule-based monochromatic and polychromatic OLEDs with wet-process feasibility. *Chem. Asian J.* **2013**, *8*, 2111–2124. [[CrossRef](#)]
29. Mondal, A.; Paterson, L.; Kun-Han Lin, J.C.; van der Zee, B.; Wetzelaer, G.-J.A.H.; Stankevych, A.; Vakhnin, A.; Kim, J.-J.; Kadashchuk, A.; Blom Falk May, P.W.M.; et al. Molecular library of OLED host materials—Evaluating the multiscale simulation workflow. *Chem. Phys. Rev.* **2021**, *2*, 031304. [[CrossRef](#)]
30. Kempegowda, R.M.; Malavalli, M.K.; Malimath, G.H.; Naik, L.; Manjappa, K.B. Synthesis and Photophysical Properties of Multi-Functional Bisimidazolyl Phenol Zinc (II) Complex: Application in OLED, Anti-Counterfeiting and Latent Finger Print Detection. *ChemistrySelect* **2021**, *6*, 3033–3039. [[CrossRef](#)]
31. Sheldrick, G.M. *SADABS, Empirical Absorption Correction Program*; Bruker AXS Inc.: Madison, WI, USA, 1997; p. 27.

32. Sheldrick, G.M. SHELXT—Integrated space-group and crystal-structure determination. *Acta Crystallogr. Sect. A Found. Adv.* **2015**, *71*, 3–8. [[CrossRef](#)]
33. Dolomanov, O.V.; Bourhis, L.J.; Gildea, R.J.; Howard, J.A.; Puschmann, H. OLEX2: A complete structure solution, refinement and analysis program. *J. Appl. Crystallogr.* **2009**, *42*, 339–341. [[CrossRef](#)]

Disclaimer/Publisher’s Note: The statements, opinions and data contained in all publications are solely those of the individual author(s) and contributor(s) and not of MDPI and/or the editor(s). MDPI and/or the editor(s) disclaim responsibility for any injury to people or property resulting from any ideas, methods, instructions or products referred to in the content.